PROCEEDINGS OF SCIENCE

PoS(ICRC2025)599

Long-term multiwavelength view and modeling of the blazar B2 1811+31 in high state

D. Cerasole[a,b,*] **and S. Loporchio**[a,b] **on behalf of the MAGIC and Fermi-LAT Collaborations, and on behalf of multiwavelength collaborators**

[a] *Istituto Nazionale di Fisica Nucleare, Sezione di Bari, 70126 Bari, Italy*
[b] *Dipartimento di Fisica 'M. Merlin' dell'Università e del Politecnico di Bari, 70126 Bari, Italy*

E-mail: `davide.cerasole@ba.infn.it`

Intermediate synchrotron-peaked BL Lacs (IBLs) are quite rare sources in the very high-energy (VHE; 100 GeV $< E <$ 100 TeV) γ-ray sky. The IBL B2 1811+31 ($z = 0.117$) showed intense flaring activity in 2020. This event was detected by a wide range of multiwavelength (MWL) instruments from radio up to γ rays. The observations carried out by the MAGIC telescopes led to the first-time detection of VHE γ-ray emission from B2 1811+31.

In this contribution, we highlight the key results of our recent study [1], which offers a comprehensive analysis of the source emission both during the 2020 high-activity state and during the quiescent state. Using a comprehensive MWL dataset, we contextualize this high-state episode within the source emissions over 18 years, from 2005 to 2024. We attribute the VHE γ-ray emission and the spectral and variability properties in the X-ray band to the electrons and positrons accelerated at the highest energies in the jet of the source. We propose a leptonic two-zone self-consistent model to interpret the observed MWL emission during the 2020 flaring state.

39th International Cosmic Ray Conference (ICRC2025)
15–24 July 2025
Geneva, Switzerland

---

[*] Speaker

1. Introduction

Blazars are a subclass of active galactic nuclei (AGNs) characterized by relativistic jets directed nearly along our line of sight. At their core lies a supermassive black hole, typically with a mass of $10^7 - 10^9$ solar masses, which is fueled by matter accreting from a surrounding disk. Despite representing only a small fraction of astrophysical sources observed in the optical range, blazars dominate the population of objects detected at γ-ray energies.

Most of the observational properties of blazars derive from their jets hosting components streaming at relativistic speeds along the jet, as revealed by imaging at radio frequencies, and hosting efficient acceleration of particles up to relativistic energies. Thanks to these properties, the radiation observed from Earth is boosted by beaming and Doppler effects, making blazars ubiquitous in the γ-ray sky. The broadband spectral energy distribution (SED) of blazars is typically composed by a nonthermal continuum showing two main components [e.g., 2]. The low energy component, peaking between the infrared and X-ray bands, is generally attributed to synchrotron emission from relativistic electrons within the jet. The high energy component, which peaks at energies above a few mega-electronvolts, is widely interpreted as resulting from inverse Compton (IC) scattering. The seed photons for this process can originate from the synchrotron radiation produced by the same electron population, in the synchrotron self-Compton (SSC) models, or from external sources such as the broad-line region and the accretion disk. A subdominant hadronic component may also be present, as discussed in [3], and supported by the indication of neutrino emission from active galaxies [e.g., 4].

Blazars are categorized based on the characteristics of their optical/UV spectra into two main classes: flat spectrum radio quasars (FSRQs), which exhibit prominent emission lines, and BL Lacertae objects (BL Lacs), which show weak or no emission lines. BL Lacs are further subdivided according to the frequency of their synchrotron peak, ν_s, into three types: low-frequency-peaked BL Lacs (LBLs, $\nu_\mathrm{s} < 10^{14}, \mathrm{Hz}$), intermediate-frequency-peaked BL Lacs (IBLs, $10^{14}, \mathrm{Hz} < \nu_\mathrm{s} < 10^{15}, \mathrm{Hz}$), and high-frequency-peaked BL Lacs (HBLs, $\nu_\mathrm{s} > 10^{15}, \mathrm{Hz}$). The majority of blazars detected in the VHE band are HBLs, while VHE-detected IBLs remain relatively rare.

The IBL B2 1811+31 ($z = 0.117$) entered the Olympus of the sources detected at VHE γ rays in 2020, thanks to the observations carried out by the Major Atmospheric Gamma-ray Imaging Cherenkov (MAGIC) telescopes [5] in a period of high state primarily detected by the the Large Area Telescope (LAT) on board the *Fermi Gamma-Ray Space Telescope* in the high-energy (HE; $100\,\mathrm{MeV} < \mathrm{E} < 100\,\mathrm{GeV}$) γ-ray band [6]. The multiwavelength observational campaign also included instruments onboard the *Neil Gehrels Swift Observatory*, covering the optical-to-X-ray range, along with several ground-based optical and radio telescopes.

In this work, we included a comprehensive MWL dataset spanning from 2005 up to 2024, with a particular focus on the data collected during the 2020 high state, from radio to VHE γ rays. Section 2 is dedicated to present the MWL dataset, along with the analyses aimed at characterizing the variability and correlations of the source emission. In Section 3, we present a leptonic modeling of the radiative state during the 2020 VHE flare period and discuss its consistence given the main dynamical processes for the electrons and positrons in the emission regions dominating the blazar emission. We summarize our results and present our conclusions in Section 4.

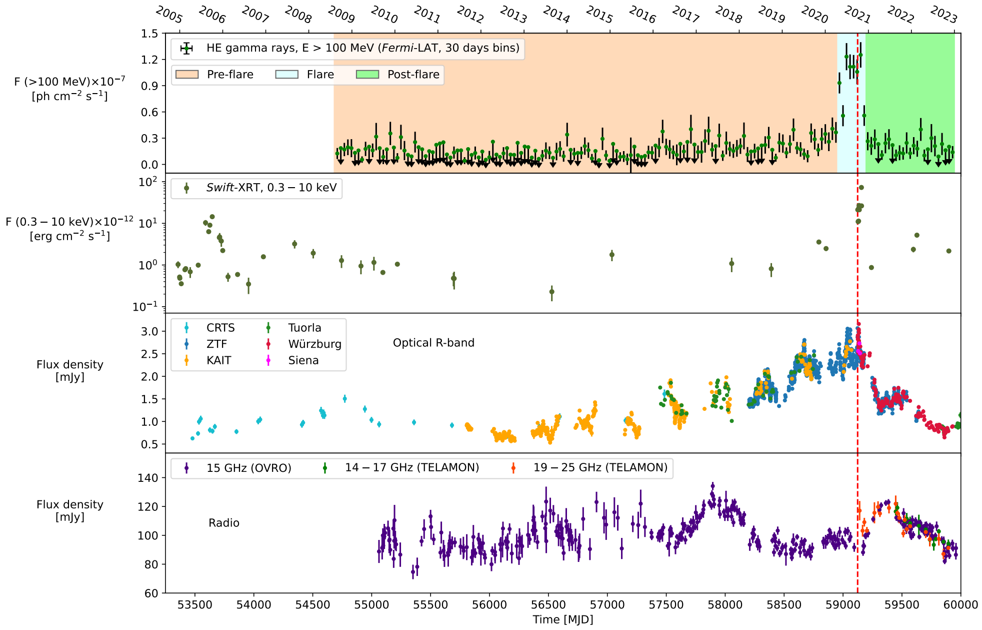

Figure 1: B2 1811+31 lightcurve collected from 2005 to 2023. *From top to bottom panels*: HE γ-ray flux above 100 MeV from *Fermi*-LAT monthly data, X-ray flux at $0.3-10$ keV from *Swift*-XRT, optical R-band data and radio data. The dashed red line marks the *Fermi*-LAT high-state detection on October 1, 2020 (MJD 59123). The shaded light orange, light blue, and green bands in the top panel indicate the "Pre-flare", "Flare" and "Post-flare" periods, respectively. Image taken from [1], licensed under CC BY 4.0.

2. The history of the long-term multiwavelength emission of B2 1811+31

The long-term multiwavelength lightcurve of B2 1811+31over 18 years from 2005 up to 2023 is shown in Figure 1. For the details of the data analysis for each instrument, the reader is addressed to Section 2 of [1]. Figure 1 shows that in 2020 the source exhibited a high state in HE γ rays, in X rays and in the optical/UV band. In addition, we found the long-term evolution of the HE γ-ray and optical R-band emission to be correlated with a significance above 95%. Conversely, the long-term radio lightcurve collected with the 40 m Telescope of the Owens Valley Radio Observatory [OVRO, 7] shows a trend that is uncorrelated with the lightcurves at higher frequencies. Therefore, the bulk of the radio emission is likely originated in regions located further along the jet than those responsible for the emission at higher frequencies. Indeed, the jet regions dominating the output at higher frequencies are likely located closer to the central engine and their GHz radio emission is suppressed due to synchrotron self-absorption.

The long-term optical light curve reveals that the 2020 high state took place at the peak of a multi-year increasing trend in the optical band, which began around 2015–2016. Following this high-state episode, the optical flux declined with a decay timescale significantly shorter than that of the preceding rising phase leading up to the 2020 peak. The long-term evolution in the γ-ray band shows a similar pattern, characterized by a rise, peak, and subsequent decline. In addition, the optical R-band and HE γ-ray light-curves showed correlated rising and falling trends in 2020 (see Figure 2 in [1]), with characteristic timescales of $\approx$ 10 days.

Figure 2 presents a close-up view of the multiwavelength lightcurve over a 70-day interval

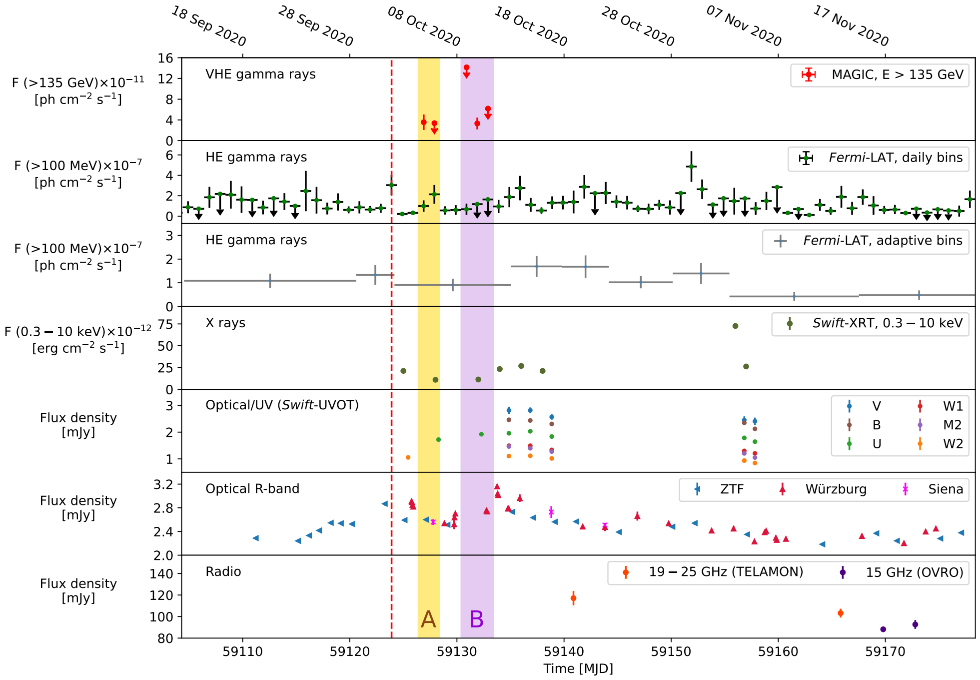

Figure 2: Lightcurve of B2 1811+31 in approximately 70 days surrounding the *Fermi*-LAT high-state detection on MJD 59123, marked by the dashed red line. *From top to bottom panels*: VHE γ-ray flux above 135 GeV from MAGIC, HE γ-ray flux above 100 MeV from *Fermi*-LAT in daily bins and using the 'adaptive-binning' method, X-ray flux in the $0.3-10\,$keV range from *Swift*-XRT, optical/UV data from *Swift*-UVOT, optical R-band data and radio data. Image taken from [1].

encompassing the MAGIC observations. Inspection of the daily HE γ-ray lightcurve allowed us to estimate a variability timescale $t_{\rm var} \approx (3-6)$ h. Using a causality argument, we employed this variability timescale estimate to constrain the size of the emission region dominating the γ-ray flux to be smaller than $\mathrm{R}_{\rm max} \approx (3-6)\times 10^{14}\,\delta_{\rm D}$ cm, where $\delta_{\rm D}$ is the region relativistic Doppler factor[1].

The broadband spectral properties of B2 1811+31 during the 2020 high state appear to differ significantly from those during the quiescent state. During the high state, we detected a significant shift to higher frequencies and higher flux levels in the synchrotron bump. While the low-state classification is compatible with an IBL behavior, showing synchrotron peak frequency $\nu_{\rm s} = 10^{14.71\pm0.03}$ Hz, the high-state classification is borderline between IBL and HBL, as the reconstructed $\nu_{\rm s} = 10^{15.21\pm0.23}$ Hz is slightly above 10^{15} Hz.

The long-term evolution of the B2 1811+31 SED in the optical/UV band and in $0.3-10\,$keV X-ray energy range is shown in the left panel of Figure 3. The optical/UV band hosts the synchrotron bump peak, whereas the X-ray band hosts the falling segment of the synchrotron bump. During the 2020 high state, higher X-ray fluxes and harder X-ray spectra are detected and a variability in the X-ray flux by more than 2 orders of magnitude at 10^{18} Hz is observed. This variability is a direct expression of the variability in the amount of the highest energy electrons accelerated in

---

[1] Consider two inertial frames S and S′, with S′ moving at velocity $\vec{v} = \vec{\beta}c$ relative to S. A photon having energy ϵ in S and moving at angle θ from $\vec{v}$, in S′ has energy $\epsilon' = \epsilon/\delta_{\rm D}$, with $\delta_{\rm D} = \Gamma^{-1}\,(1-\beta\cos\theta)^{-1}$ and $\Gamma = \left(1-\beta^2\right)^{-1/2}$.

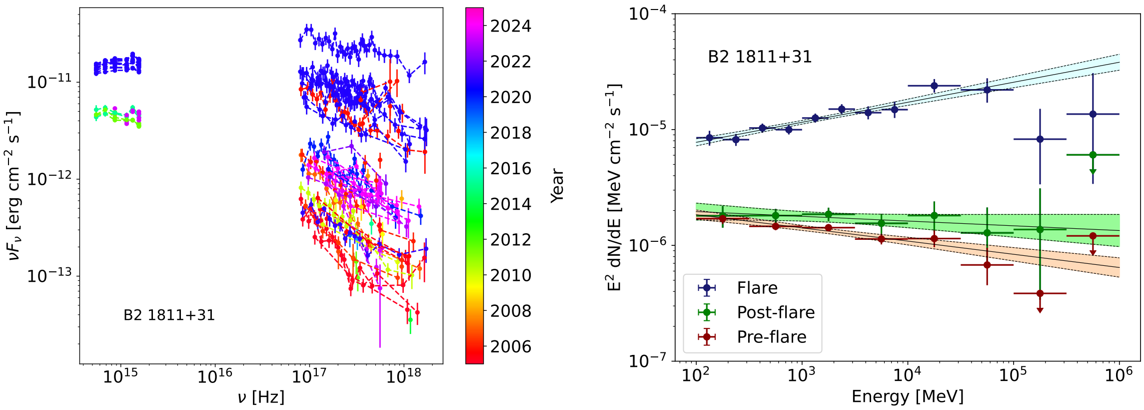

Figure 3: *Left panel*: Long-term evolution of the optical-to-X-ray SED of B2 1811+31 reconstructed from the *Swift*-UVOT and *Swift*-XRT observations. *Right panel*: SED in the 100 MeV – 1 TeV energy range resulting from *Fermi*-LAT data from the "Pre-flare" (red), "Flare" (blue) and "Post-flare" (green) periods. Images taken from [1].

the jet. In addition, a power law spectrum of electrons $n_e(\gamma) \propto \gamma^{-p}$ radiates a synchrotron SED $\nu F_{\nu,\mathrm{synch}} \propto \nu^{\frac{3-p}{2}}$. Therefore, since during the MAGIC observation period the X-ray SED slope is $\Gamma_X = 2.58 \pm 0.10$, we estimate a spectral slope of the electrons dominating the X-ray flux equal to $p_2 = 2\Gamma_X - 1 \approx 4.2 \pm 0.2$.

The right panel of Figure 3 shows that in the HE γ-ray band the source experienced an average flux enhancement by a factor of ~ 6 compared to the average radiative states before and after the 2020 flare, as well as a strong spectral hardening, with photon index changing from 2.11 ± 0.03 in low state to 1.83 ± 0.02 in high state. These evidence indicate that the spectral break of the HE bump shifted from below hundreds of MeV during the quiescent state to about tens of GeV during the high state.

All these multiwavelength evidence related to the comparison between the quiescent state and the 2020 high state indicate that, during the high activity state, the particle spectrum accelerated in the jet was subject to an average hardening and brightening compared to the low state period. Additional contributions to the observed brighter and harder spectra may derive from the presence of enhanced magnetic fields in the jet, as well as higher bulk Lorentz factor and closer alignment with our line of sight, enhancing the Doppler-boosting and beaming effects.

We analysed the correlations between the flux and spectral index of the X-ray and HE γ-ray emission within each activity state independently (see Figure 6 in [1]). We found that the X-ray spectrum was subject to a significant harder-when-brighter trend also within each of the high and low state. This is interpreted as resulting from the acceleration of electrons and positrons and from synchrotron cooling being more effective with increasing particle energy, since $\left(\frac{d\gamma}{dt}\right)_{\mathrm{synch}} \propto -\gamma^2$. Indeed, while acceleration mechanisms result in the injection of particles in the emission regions with a hard spectrum, e.g., $\frac{dN}{d\gamma} \propto \gamma^{-2}$ from first-order Fermi acceleration, synchrotron emission proceeds in cooling faster the high-energy tail of the particle spectrum than the particles with lower energies, therefore softening the spectrum at high energies and reducing the X-ray flux.

Conversely, we found a hint of a softer-when-brighter behaviour in the HE γ-ray band (see

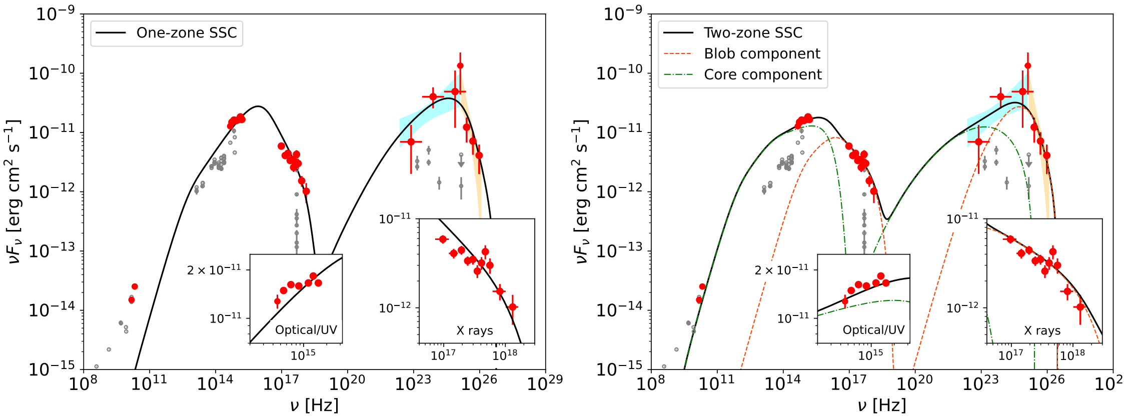

Figure 4: Leptonic one-zone (*left panel*) and two-zone (*right panel*) SSC modeling of the broadband SED of B2 1811+31 within the 2020 high state in VHE γ rays, marked by the red points. Archival data are indicated by the hollow gray points. The two insets show a zoom-in on the optical/UV and X-ray bands, respectively. Images from [1].

Table 1: SED modeling parameters for the one-zone and two-zone SSC model of the 2020 VHE γ-ray high state of B2 1811+31. Columns: (1) Model. (2), (3), (4) Minimum, break and maximum electron Lorentz factors. (5), (6) Slopes of the electron spectrum around the break. (7) Magnetic field strength. (8) Electron density. (9) Radius of the emission region. (10) Doppler factor. (11) Equipartition parameter.

Model (region)	$\gamma_{\rm min}$ [$\times10^3$]	$\gamma_{\rm b}$ [$\times10^4$]	$\gamma_{\rm max}$ [$\times10^5$]	p_1	p_2	B [G]	K_e [cm^{-3}]	$R_{\rm b}$ [$\times10^{15}$cm]	$\delta_{\rm D}$	u_e/u_B
One-zone	0.7	3.2	3.0	1.9	4.4	0.13	7.6	10.6	20	31.3
Two-zone (blob)	6.0	4.0	3.0	2.0	3.8	0.38	7.95	4.0	10	18.3
Two-zone (core)	0.5	0.38	0.7	1.8	2.7	0.17	0.74	210	4	1.0

Figure 7 in [1]) both within the quiescent and flare periods. In both periods, the radiation in this band is emitted by particles in the energy region corresponding to the break of the particle spectrum. Although this is not the first indication of softer-when-brighter trends in the spectral evolution at HE γ rays of a blazar [9, e.g.,], the interpretation of this effect is still unclear. Standard acceleration mechanisms are expected to yield harder-when-brighter trends instead. One possibility is that softer-when-brighter trends may result from the total HE γ-ray flux being the compositions of different emission components (e.g., SSC and EC) or diverse emission regions. However, a quantitative analysis of this scenario is outside the scope of the current work.

3. The modeling of the 2020 high state seen with MAGIC

Blazar jets efficiently accelerate particles through several distinct mechanisms. These include magnetic reconnection, first-order Fermi acceleration at relativistic shocks—such as internal or recollimation shocks, stochastic and second-order Fermi acceleration. In parallel, the accelerated particles are subject to both radiative and non-radiative cooling processes. Electrons, in particular, lose energy radiatively via synchrotron emission and IC scattering of ambient low-energy photons. In BL Lacs, the intensity of photon fields external to the jet, such as from the accretion disk, is

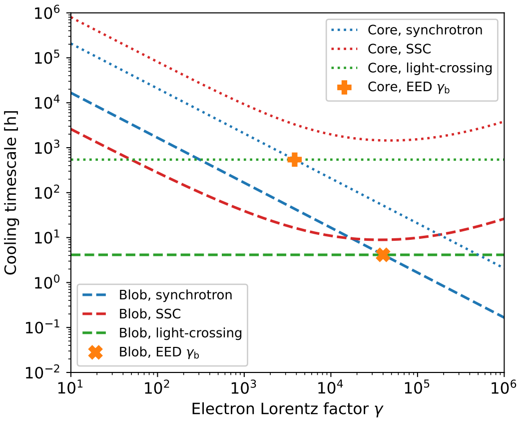

Figure 5: Competition among the cooling timescales for the two-zone model in Figure 4, as a function of the electron Lorentz factor γ. Dashed (dotted) curves refer to the blob (core) region. The orange markers indicate the spectral breaks of the particle distributions within the two emission regions. Image from [1].

thought to be negligible with respect to the synchrotron radiation originated in the jet. For IBLs and HBLs, SSC models are typically preferred over models including external Compton components.

In the simplest scenario, the emission region is assumed to be a spherical blob populated by electrons spiraling in comoving uniform magnetic field. The blob can be imagined as an ideal emission zone which can represent a variety of relativistic plasma configurations within the jet, such as superluminal knots, recollimation shocks, or standing shocks. In order to model the broad-band spectrum of B2 1811+31 during the observational campaign with MAGIC, we tested a single-zone scenario and a two-zone SSC model. In the two-zone scenario, we consider a *blob* region as a small, fast, and energetic region dominating the flux in the X and VHE γ-ray bands. In addition, we employ a *core* region, larger and slower region than the blob, to dominate the optical/UV flux, still contributing significantly to the HE γ-ray emission. The core is supposed to be located further along the jet with respect to the blob, where the ambient jet magnetic field is expected to be lower. The results are shown in Figure 4. The size of the blob is consistent with the indications from the shortest variability in the HE γ-ray band, whereas the size of the core is comparable with the ≈ 10 days variations shown both in optical and in the *Fermi*-LAT data during 2020 (Section 2).

In the construction of the models, we investigated the possibility to account for the observed broadband SED with self-consistent particle populations in the emission regions. The temporal evolution of the particle energetic distribution is typically studied through a continuity equation under the effects of particle acceleration/injection, escape, adiabatic expansion and radiative cooling [e.g., 8]. Figure 5 shows, for the two regions presented in Figure 4, the competition among the light-crossing timescale, t_{lc}, and the main radiative cooling timescales. The light-crossing timescale can be interpreted as the characteristic time for the particle escape from the emission region. For each emission region, the SSC cooling timescale corresponds to that of the IC scattering off the (isotropic) synchrotron photon density. We considered the case of the continuity equation with a power law injection term, that is $\frac{dN}{d\gamma} \propto \gamma^{-p_1}$, with synchrotron and IC scattering (Thomson limit only) being the main radiative cooling mechanisms, and with particle escape with timescale t_{lc}. The steady-state solution of this equation is a broken power law having indices p_1 and p_2, with spectral break $p_2 - p_1 = 1$, and γ_b equal to the value of γ at which the escape and radiative cooling timescales coincide [e.g., 8]. We find that, for both regions in the two-zone model, the γ_b values in our solution (Table 1) are equal to those obtained comparing the radiative cooling timescales with t_lc. In addition, in the core region also the spectral break is found to be equal to the one expected at equilibrium. Conversely, for the blob, a harder break is necessary to account for the observed spectra. This suggests that further effects may be relevant, such as the particle distribution being hardly at equilibrium or effects related to cooling in the Klein-Nishina regime.

4. Conclusions

In this contribution, we presented a long-term MWL view of B2 1811+31, with the main emphasis given to the 2020 γ-ray flare of the source. During this high-state period, the MAGIC telescopes reported the first-time detection of VHE γ-ray emission from the source. We investigated the variability, spectral features and correlations of the multiwavelength emission both in the quiescent and flaring states. In addition, we modeled the broad-band SED observed during the observational campaign that MAGIC joined in a leptonic SSC scenario. The proposed two-zone model describes well the MWL emission and is compatible with the expectations from the temporal evolution of the particle distribution under the effects of injection, escape and radiative losses.

Acknowledgments

We would like to thank the Instituto de Astrofísica de Canarias for the excellent working conditions at the Observatorio del Roque de los Muchachos in La Palma. The financial support of the German BMBF, MPG and HGF; the Italian INFN and INAF; the Swiss National Fund SNF; the grants PID2019-107988GB-C22, PID2022-136828NB-C41, PID2022-137810NB-C22, PID2022-138172NB-C41, PID2022-138172NB-C42, PID2022-138172NB-C43, PID2022-139117NB-C41, PID2022-139117NB-C42, PID2022-139117NB-C43, PID2022-139117NB-C44, CNS2023-144504 funded by the Spanish MCIN/AEI/ 10.13039/501100011033 and "ERDF A way of making Europe; the Indian Department of Atomic Energy; the Japanese ICRR, the University of Tokyo, JSPS, and MEXT; the Bulgarian Ministry of Education and Science, National RI Roadmap Project DO1-400/18.12.2020 and the Academy of Finland grant nr. 320045 is gratefully acknowledged. This work was also been supported by Centros de Excelencia "Severo Ochoa" y Unidades "María de Maeztu" program of the Spanish MCIN/AEI/ 10.13039/501100011033 (CEX2019-000920-S, CEX2019-000918-M, CEX2021-001131-S) and by the CERCA institution and grants 2021SGR00426 and 2021SGR00773 of the Generalitat de Catalunya; by the Croatian Science Foundation (HrZZ) Project IP-2022-10-4595 and the University of Rijeka Project uniri-prirod-18-48; by the Deutsche Forschungsgemeinschaft (SFB1491) and by the Lamarr-Institute for Machine Learning and Artificial Intelligence; by the Polish Ministry Of Education and Science grant No. 2021/WK/08; and by the Brazilian MCTIC, CNPq and FAPERJ. This research has made use of data from the OVRO 40-m monitoring program [7], supported by private funding from the California Institute of Technology and the Max Planck Institute for Radio Astronomy, and by NASA grants NNX08AW31G, NNX11A043G, and NNX14AQ89G and NSF grants AST-0808050 and AST-1109911. The *Fermi*-LAT Collaboration acknowledges support for LAT development, operation and data analysis from NASA and DOE (United States), CEA/Irfu and IN2P3/CNRS (France), ASI and INFN (Italy), MEXT, KEK, and JAXA (Japan), and the K.A. Wallenberg Foundation, the Swedish Research Council and the National Space Board (Sweden). Science analysis support in the operations phase from INAF (Italy) and CNES (France) is also gratefully acknowledged. This work performed in part under DOE Contract DE-AC02-76SF00515. This work has made use of data from the Joan Oró Telescope (TJO) of the Montsec Observatory (OdM), which is owned by the Catalan Government and operated by the Institute for Space Studies of Catalonia (IEEC). This work is based on observations with the 100-m telescope of the MPIfR (Max-Planck-Institut für Radioastronomie) at Effelsberg.

References

[1] K. Abe et al., *Very high-energy gamma-ray detection and long-term multiwavelength view of the flaring blazar B2 1811+31*, A&A, 697, A172 (2025)

[2] Ghisellini, G. et al., MNRAS, 469, 255 (2017)

[3] Murase, K., Dermer, C. D., Takami, H., Migliori, G., ApJ, 749, 63 (2012)

[4] Aartsen, M. G., Ackermann, M., et al., Science, 361, 147, eaat1378 (2018)

[5] Blanch O., The Astronomer's Telegram, No. 14090. (2020)

[6] Angioni R., Bissaldi E., Garrappa S., Longo F., Kocevski D., The Astronomer's Telegram, No. 14060. (2020)

[7] Richards, J. L., Max-Moerbeck, W., Pavlidou, V., et al. 2011, ApJS, 194, 29

[8] Kardashev, N. S. 1962, Soviet Ast., 6, 3171619

[9] Prince, R. et al. 2022, MNRAS, 515, 2633

[10] J.S Chang, G Cooper, Journal of Computational Physics, Volume 6, Issue 1, Pages 1-16 (1970)

PoS(ICRC2025)599

Full Author List

K. Abe[1], S. Abe[2], J. Abhir[3], A. Abhishek[4], V. A. Acciari[5], A. Aguasca-Cabot[6], I. Agudo[7], T. Aniello[8] , S. Ansoldi[9,42], L. A. Antonelli[8], A. Arbet Engels[10], C. Arcaro[11], K. Asano[2], A. Babić[12], U. Barres de Almeida[13], J. A. Barrio[14], L. Barrios-Jiménez[15], I. Batković[11], J. Baxter[2] , J. Becerra González[15], W. Bednarek[16], E. Bernardini[11], J. Bernete[17], A. Berti[10], J. Besenrieder[10], C. Bigongiari[8], A. Biland[3], O. Blanch[5], G. Bonnoli[8], Ž. Bošnjak[12], E. Bronzini[8] , I. Burelli[5], A. Campoy-Ordaz[18], A. Carosi[8], R. Carosi[19], M. Carretero-Castrillo[6], A. J. Castro-Tirado[7], D. Cerasole[20,∗], G. Ceribella[10], A. Chilingarian[21], A. Cifuentes[17], E. Colombo[5], J. L. Contreras[14], J. Cortina[17], S. Covino[8], F. D'Ammando[49], G. D'Amico[22], P. Da Vela[8], F. Dazzi[8], A. De Angelis[11], B. De Lotto[9], R. de Menezes[23] , M. Delfino[5,43], J. Delgado[5,43], C. Delgado Mendez[17], F. Di Pierro[23], R. Di Tria[20] , L. Di Venere[20], A. Dinesh[14] , D. Dominis Prester[24], A. Donini[8], D. Dorner[25], M. Doro[11], L. Eisenberger[25] , D. Elsaesser[26,57], J. Escudero[7], L. Fariña[5], L. Foffano[8], L. Font[18], S. Fröse[26] , Y. Fukazawa[27], R. J. García López[15], M. Garczarczyk[28], S. Gasparyan[29], M. Gaug[18], J. G. Giesbrecht Paiva[13], N. Giglietto[20], F. Giordano[20], P. Gliwny[16], T. Gradetzke[26] , R. Grau[5], D. Green[10], J. G. Green[10], P. Günther[25] , D. Hadasch[2], A. Hahn[10], T. Hassan[17], L. Heckmann[10,44], J. Herrera Llorente[15], D. Hrupec[30], R. Imazawa[27], D. Israyelyan[29], T. Itokawa[2] , I. Jiménez Martínez[10], J. Jiménez Quiles[5] , J. Jormanainen[31], S. Kankkunen[31] , T. Kayanoki[27] , D. Kerszberg[5], M. Khachatryan[29] , G. W. Kluge[22,45], Y. Kobayashi[2], J. Konrad[26] , P. M. Kouch[31] , H. Kubo[2], J. Kushida[1], M. Láinez[14], A. Lamastra[8], E. Lindfors[31], S. Lombardi[8], F. Longo[9,46], R. López-Coto[7], M. López-Moya[14], A. López-Oramas[15], S. Loporchio[20,∗], A. Lorini[4] , L. Lulić[24] , E. Lyard[32] , P. Majumdar[33], M. Makariev[34], G. Maneva[34], M. Manganaro[24], S. Mangano[17], K. Mannheim[25,56], M. Mariotti[11], M. Martínez[5], P. Maruševec[12] , A. Mas-Aguilar[14], D. Mazin[2,47], S. Menchiari[7] , S. Mender[26], D. Miceli[11], J. M. Miranda[4], R. Mirzoyan[10], M. Molero González[15] , E. Molina[15], H. A. Mondal[33], A. Moralejo[5], T. Nakamori[35], C. Nanci[8], V. Neustroev[36], L. Nickel[26] , M. Nievas Rosillo[15], C. Nigro[5], L. Nikolić[4] , K. Nilsson[31], K. Nishijima[1], T. Njoh Ekoume[5], K. Noda[37], S. Nozaki[10], A. Okumura[38] , S. Paiano[8], D. Paneque[10], R. Paoletti[4], J. M. Paredes[6], L. Pavletić[24,∗], M. Peresano[10], M. Persic[9,48], M. Pihet[6], G. Pirola[10] , F. Podobnik[4], P. G. Prada Moroni[19], E. Prandini[11], G. Principe[9], W. Rhode[26], M. Ribó[6], J. Rico[5], C. Righi[8], N. Sahakyan[29], T. Saito[2], F. G. Saturni[8], K. Schmitz[26] , F. Schmuckermaier[10], J. L. Schubert[26] , A. Sciaccaluga[8] , G. Silvestri[11] , J. Sitarek[16], V. Sliusar[32], D. Sobczynska[16], A. Stamerra[8], J. Strišković[30], D. Strom[10], M. Strzys[2], Y. Suda[27] , H. Tajima[38] , M. Takahashi[38], R. Takeishi[2], P. Temnikov[34], K. Terauchi[39] , T. Terzić[24], M. Teshima[10,1] , A. Tutone[8], S. Ubach[18], J. van Scherpenberg[10], M. Vazquez Acosta[15] , S. Ventura[4], G. Verna[4] , I. Viale[11], A. Vigliano[9] , C. F. Vigorito[23], V. Vitale[40], I. Vovk[2], R. Walter[32], F. Wersig[26] , M. Will[10], T. Yamamoto[41], C. Bartolini[66,59], E. Bissaldi[58,59], S. Garrappa[60], E. Ankara[55] , N. Bader[55] , M. Feige[55] , F. Hümmer[55] , F. Kaplan[55] , C. Lorey[55], D. Reinhart[55] , K. Schoch[55] , R. Steineke[55] , A. Marchini[54], V. Fallah Ramazani[63], M. J. Graham[65], T. Hovatta[63,64], S. Kiehlmann[50], A. C. S. Readhead[50,51], P. Benke[53,52], F. Eppel[52,53], S. Hämmerich[62], J. Heßdörfer[52,53], M. Kadler[52], D. Kirchner[52] , A. Gokus[61,62,52], G. F. Paraschos[53], F. Rösch[52,53], J. Sinapius[28].

[1] Japanese MAGIC Group: Department of Physics, Tokai University, Hiratsuka, 259-1292 Kanagawa, Japan, [2] Japanese MAGIC Group: Institute for Cosmic Ray Research (ICRR), The University of Tokyo, Kashiwa, 277-8582 Chiba, Japan, [3] ETH Zürich, CH-8093 Zürich, Switzerland, [4] Università di Siena and INFN Pisa, I-53100 Siena, Italy, [5] Institut de Física d'Altes Energies (IFAE), The Barcelona Institute of Science and Technology (BIST), E-08193 Bellaterra (Barcelona), Spain, [6] Universitat de Barcelona, ICCUB, IEEC-UB, E-08028 Barcelona, Spain, [7] Instituto de Astrofísica de Andalucía-CSIC, Glorieta de la Astronomía s/n, 18008, Granada, Spain, [8] National Institute for Astrophysics (INAF), I-00136 Rome, Italy, [9] Università di Udine and INFN Trieste, I-33100 Udine, Italy, [10] Max-Planck-Institut für Physik, D-85748 Garching, Germany, [11] Università di Padova and INFN, I-35131 Padova, Italy, [12] Croatian MAGIC Group: University of Zagreb, Faculty of Electrical Engineering and Computing (FER), 10000 Zagreb, Croatia, [13] Centro Brasileiro de Pesquisas Físicas (CBPF), 22290-180 URCA, Rio de Janeiro (RJ), Brazil, [14] IPARCOS Institute and EMFTEL Department, Universidad Complutense de Madrid, E-28040 Madrid, Spain, [15] Instituto de Astrofísica de Canarias and Dpto. de Astrofísica, Universidad de La Laguna, E-38200, La Laguna, Tenerife, Spain, [16] University of Lodz, Faculty of Physics and Applied Informatics, Department of Astrophysics, 90-236 Lodz, Poland, [17] Centro de Investigaciones Energéticas, Medioambientales y Tecnológicas, E-28040 Madrid, Spain, [18] Departament de Física, and CERES-IEEC, Universitat Autònoma de Barcelona, E-08193 Bellaterra, Spain, [19] Università di Pisa and INFN Pisa, I-56126 Pisa, Italy, [20] INFN MAGIC Group: INFN Sezione di Bari and Dipartimento Interateneo di Fisica dell'Università e del Politecnico di Bari, I-70125 Bari, Italy, [21] Armenian MAGIC Group: A. Alikhanyan National Science Laboratory, 0036 Yerevan, Armenia, [22] Department for Physics and Technology, University of Bergen, Norway, [23] INFN MAGIC Group: INFN Sezione di Torino and Università degli Studi di Torino, I-10125 Torino, Italy, [24] Croatian MAGIC Group: University of Rijeka, Faculty of Physics, 51000 Rijeka, Croatia, [25] Universität Würzburg, D-97074 Würzburg, Germany, [26] Technische Universität Dortmund, D-44221 Dortmund, Germany, [27] Japanese MAGIC Group: Physics Program, Graduate School of Advanced Science and Engineering, Hiroshima University, 739-8526 Hiroshima, Japan, [28] Deutsches Elektronen-Synchrotron (DESY), D-15738 Zeuthen, Germany, [29] Armenian MAGIC Group: ICRANet-Armenia, 0019 Yerevan, Armenia, [30] Croatian MAGIC Group: Josip Juraj Strossmayer University of Osijek, Department of Physics, 31000 Osijek, Croatia, [31] Finnish MAGIC Group: Finnish Centre for Astronomy with ESO, Department of Physics and Astronomy, University of Turku, FI-20014 Turku, Finland, [32] University of Geneva, Chemin d'Ecogia 16, CH-1290 Versoix, Switzerland, [33] Saha Institute of Nuclear Physics, A CI of Homi Bhabha National Institute, Kolkata 700064, West Bengal, India, [34] Inst. for Nucl. Research and Nucl. Energy, Bulgarian Academy of Sciences, BG-1784 Sofia, Bulgaria, [35] Japanese MAGIC Group: Department of Physics, Yamagata University, Yamagata 990-8560, Japan, [36] Finnish MAGIC Group: Space Physics and Astronomy Research Unit, University of Oulu, FI-90014 Oulu, Finland, [37] Japanese MAGIC Group: Chiba University, ICEHAP, 263-8522 Chiba, Japan, [38] Japanese MAGIC Group: Institute for Space-Earth Environmental Research and Kobayashi-Maskawa Institute for the Origin of Particles and the Universe, Nagoya University, 464-6801 Nagoya, Japan, [39] Japanese MAGIC Group: Department of Physics, Kyoto University, 606-8502 Kyoto, Japan, [40] INFN MAGIC Group: INFN Roma Tor Vergata, I-00133 Roma, Italy, [41] Japanese MAGIC Group: Department of Physics, Konan University, Kobe, Hyogo 658-8501, Japan, [42] also at International Center for Relativistic Astrophysics (ICRA), Rome, Italy, [43] also at Port d'Informació Científica (PIC), E-08193 Bellaterra (Barcelona), Spain, [44] now at Université Paris Cité, CNRS, Astroparticule et Cosmologie, F-75013 Paris, France, [45] also at Department of Physics, University of Oslo, Norway, [46] also at Dipartimento di Fisica, Università di Trieste, I-34127 Trieste, Italy, [47] Max-Planck-Institut für Physik, D-85748 Garching, Germany, [48] also at INAF Padova, [49] INAF Istituto di Radioastronomia, Via P. Gobetti 101, 40129 Bologna, Italy, [50] Institute of Astrophysics, Foundation for Research and Technology-Hellas, GR-71110 Heraklion, Greece, [51] Owens Valley Radio Observatory, California Institute of Technology, Pasadena, CA 91125, USA, [52] Julius-Maximilians-Universität Würzburg, Fakultät für Physik und Astronomie, Institut für Theoretische Physik und Astrophysik, Lehrstuhl für Astronomie, Emil-Fischer-Straße 31, D-97074 Würzburg, Germany, [53] Max-Planck-Institut für Radioastronomie, Auf dem Hügel 69, D-53121 Bonn, Germany, [54] University of Siena, Department of Physical Sciences, Earth and Environment, Astronomical Observatory, Via Roma 56, 53100 Siena, Italy, [55] Hans-Haffner-Sternwarte (Hettstadt), Naturwissenschaftliches Labor für Schüler am FKG, Friedrich-Koenig-Gymnasium, D-97082 Würzburg, Germany, [56] Lehrstuhl für Astronomie, Universität Würzburg, D-97074 Würzburg, Germany, [57] Astroteilchenphysik, TU Dortmund, Otto-Hahn-Str. 4A, D-44227 Dortmund, Germany, [58] Dipartimento di Fisica "M. Merlin" dell'Università e del Politecnico di Bari, via Amendola 173, I-70126 Bari, Italy, [59] Istituto Nazionale di Fisica Nucleare, Sezione di Bari, I-70126 Bari, Italy, [60] Department of Particle Physics and Astrophysics, Weizmann Institute of Science, 76100 Rehovot, Israel, [61] Department of Physics and McDonnell Center for the Space Sciences, Washington University in St. Louis, One Brookings Drive,, St. Louis 63130, USA [62] Remeis Observatory and Erlangen Centre for Astroparticle Physics, Universität Erlangen-Nürnberg, Sternwartstr. 7, 96049 Bamberg, Germany, [63] Finnish Center for Astronomy with ESO (FINCA), Quantum, Vesilinnantie 5, FI-20014 University of Turku, Finland, [64] Aalto University Metsähovi Radio Observatory, Metsähovintie 114, 02540 Kylmälä, Finland, [65] Division of Physics, Mathematics and Astronomy, California Institute of Technology, Pasadena, CA91125, USA, [66] University of Trento, 38123, Trento, Italy,